Pathology of tumors of the nervous system. 5th ed, Baltimore: Williams and Wilkins; 1989.
25. Burger PC, Dubois PJ, Schold SC, Smith KR, Oblon GL, Grafts DC, Giangaspero F. Computerized tomographic and pathologic studies of the untreated, quiescent and recurrent glioblastoma multiforme. *J Neurosurg* 1983;58:159–169.
26. Di Chiro G, Oldfield E, Wright DC, De Michele D, Katz D, Patronas NJ, et al. Cerebral necrosis after radiotherapy and/or intraarterial chemotherapy for brain tumors: PET and neuropathologic studies. *Am J Neuroradiol* 1987;8:1083–1091.
27. Earnest F, Kelly PJ, Scheithauer BW, Kall BA, Cascino TL, Ehman RL, Forbes GS, Axley PL. Cerebral astrocytomas: histopathologic correlation of MR and CT contrast enhancement with stereotactic biopsy. *Radiology* 1988;166:823–827.
28. Mazziotta JC. The continuing challenge of primary brain tumor management: The contribution of positron emission tomography [Editorial]. *Ann Neurology* 1991;29:345–346.
29. Di Chiro G. Positron emission tomography using [^{18}F] fluorodeoxyglucose in brain tumors: powerful diagnostic and prognostic tool. *Invest Radiol* 1987;22:360–371.
30. Merboldt KD, Bruhn H, Frahm J, Gyngell ML, Hänicke W, Deimling M. MRI of "diffusion" in the human brain: New results using a modified CE-FAST sequence. *Magn Reson Med* 1989;9:423–429.
31. Tsuruda JS, Chew WM, Moseley ME, Norman D. Diffusion-weighted MR imaging of the brain: value of differentiating between extra-axial cysts and epidermoid tumors. *Am J Neuroradiol* 1990;11:925–931.
32. Chien D, Buxton RB, Kwong KK, Brady TJ, Rosen BR. MR diffusion imaging of the human brain. *J Comput Assist Tomogr* 1990;14:5114–5120.
33. Le Bihan D, Douek P, Argyropoulou M, Turner R, Patronas N, Fulham M. Diffusion and perfusion magnetic resonance imaging in brain tumors. *Top Magn Reson Imaging* 1993;5:25–31.
34. Sigal R. MR imaging for diagnosis of central nervous system cystic lesions: correlation with biochemical data. *Radiology* 1988;169(P), 423.
35. Haimes A, Zimmerman R, Morgello S, et al. MR imaging of brain abscesses. *Am J Neuroradiol* 1989;10:279–291.
36. Buchbinder BR, Belliveau JW, McKinstry RC, Asronen HJ, Kennedy DN, Cohen MS, et al. Functional MR imaging of primary brain tumors. In: *Abstracts of the proceedings of the twenty-ninth annual meeting of ANSR*. 1991:42.
37. Hooper J, Rajan S, Rosa L, Le Bihan D. Application of diffusion imaging to monitor tumor growth and response to chemotherapy. In: *Abstracts of the proceedings of the Society of Magnetic Resonance in Medicine*. Berkeley: Society of Magnetic Resonance in Medicine; 1990:371.

Chapter 8

Part II

Anisotropic Diffusion: MR Diffusion Tensor Imaging

Peter J. Basser, James Mattiello, and Denis Le Bihan

When NMR diffusion spectroscopy or imaging has been performed on heterogeneous media, such as tissues, an *apparent* diffusion constant (ADC) has been measured which depends upon tissue microdynamics and microstructure, as well as upon gradient pulse parameters. In some heterogeneous media such as gray matter, the scalar ADC is independent of the direction of the diffusion-sensitizing gradient, so that diffusion appears to be isotropic. In contrast, in other heterogeneous media, such as white matter (1) or skeletal muscle (2), the ADC depends on the direction of the diffusion-sensitizing gradient, so that diffusion appears to be anisotropic. Here, the ADC depends on the angle between the fiber-tract axis and the applied magnetic field gradient. The largest ADC is observed when the diffusion-sensitizing gradient is parallel to the fiber-tract direction and the smallest ADC is observed when the diffusion-sensitizing gradient is perpendicular to the fiber-tract direction (1–5).

In such anisotropic media, we should characterize diffusive transport by an effective diffusion *tensor*, $\underline{D}^{eff}$, rather than by a (scalar) ADC, D^{eff} (6–10). While the importance of using a tensor to describe anisotropic diffusion was already appreciated thirty years ago by Stejskal in NMR diffusion spectroscopy (11) and, more recently, in diffusion imaging (12,13), until recently, there was no method available to measure it (14). Recently, we proposed such a method that involves (i) deriving an explicit relationship between diagonal and off-diagonal elements of $\underline{D}^{eff}$ and the measured echo intensity in a pulsed-gradient, spin-echo experiment; (ii) designing a series of magnetic field gradient sequences permitting us to observe the effect of different linear combinations of the diagonal and off-diagonal elements of $\underline{D}^{eff}$ on the measured echo; and (iii) estimating $\underline{D}^{eff}$ from these experiments (14). Combining the estimation of $\underline{D}^{eff}$ with MR imaging leads to a new MR imaging modality, called diffusion *tensor* imaging, which we have used: (a) to determine orientation of organized fibrous tissues *in vivo* (15,16); (b) to infer the microscopic mean displacements and diffusivities of water (protons) *in vivo*; (c) to derive useful invariant

P. J. Basser and J. Mattiello: Biomedical Engineering and Instrumentation Program, National Center for Research Resources, National Institutes of Health, Bethesda, Maryland 20892.

D. Le Bihan: Diagnostic Radiology Department, Warren G. Magnuson Clinical Center, National Institutes of Health, Bethesda, Maryland 20892.

quantities from $\underline{D}^{eff}$ (which depend only on the composition and local microstructure of the tissue, but not on fiber direction *per se*) (15,16); and (d) to correct for cross-talk, misalignment, and maladjustment of magnetic field gradient coils.

THEORY

The Macroscopic Effective Diffusion Tensor, $\underline{D}^{eff}$

The macroscopic effective diffusion tensor $\underline{D}^{eff}$, given by

$$\underline{D}^{eff} = \begin{pmatrix} D_{xx}^{eff} & D_{xy}^{eff} & D_{xz}^{eff} \\ D_{yx}^{eff} & D_{yy}^{eff} & D_{yz}^{eff} \\ D_{zx}^{eff} & D_{zy}^{eff} & D_{zz}^{eff} \end{pmatrix}, \quad [1]$$

has two useful physical interpretations. The first is as a transport parameter that relates the macroscopic diffusive flux vector, J, and the particle concentration gradient vector, ∇C, by a generalized Fick's law appropriate for anisotropic media:

$$J = -\underline{D}^{eff} \nabla C \quad [2]$$

One important consequence of Eq. [2] is that the ∇C is not necessarily parallel to J (see Fig. 6) as it is in isotropic media. Moreover, for uncharged moieties such as water, $\underline{D}^{eff}$ must be symmetric (6–10), i.e., $\underline{D}^{eff} = (\underline{D}^{eff})T$—a requirement of the reciprocity theorem, and the principle of microscopic reversibility (of nonequilibrium thermodynamics) (8,9). The second interpretation of $\underline{D}^{eff}$ arises from considering a Brownian (random walk) model of diffusion, where $\underline{D}^{eff}$ embodies correlations between displacements along x, y, and z when the mobilities in these directions may be different. Specifically, $\underline{D}^{eff}$ appears as the covariance matrix in the conditional density function, $\rho(r \mid r_0, \tau_d)$, the probability that a particle initially at r_0 freely translates to r at time τ_d:

$$\rho(r \mid r_0, \tau_d) = \frac{1}{\sqrt{|\underline{D}^{eff}(\tau_d)| (4\pi\tau_d)^3}} \cdot \exp\left(\frac{-(r-r_0)^T \underline{D}_{eff(\tau_d)}^{-1}(r-r_0)}{4\tau_d}\right). \quad [3]$$

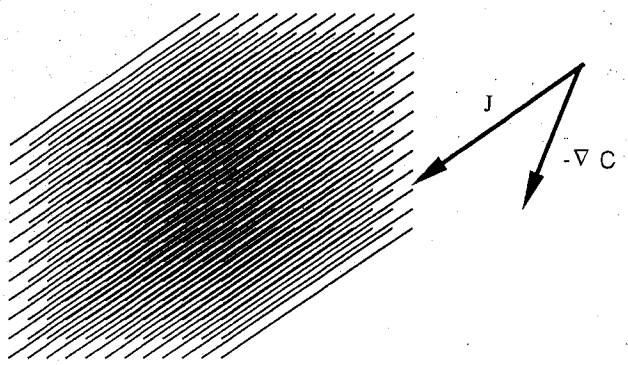

FIG. 6. A schematic diagram of an array of microscopic fiber bundles (e.g., bundles of myelinated axons) viewed at a macroscopic (voxel) length scale. At the macroscopic length scale, diffusion in this heterogeneous medium appears to be homogeneous but anisotropic. As a result, particle flux and concentration gradient vectors obey a generalized Fick's law, and are not necessarily parallel to one another.

Equations Governing the Transport of Magnetization

The Block equations (17) with diffusive transport (18) are well known, and will not be rederived here (see Chapter 1). For a pulsed-gradient sequence, it is useful to define the magnetic field gradient vector, $G(t)$,

$$G(t) = (G_x(t), G_y(t), G_z(t))^T \quad [4]$$

and its time integral,

$$k(t) = \gamma \int_0^t G(t')\, dt'. \quad [5]$$

Stejskal and Tanner derived analytic expressions relating the measured echo intensity and the applied pulsed gradient sequence for a 90°–180° spin-echo sequence (11). For isotropic media, the magnitude of the magnetization at the time of the echo, $A(TE)$, is related to the scalar self-diffusivity, D, by

$$ln\left(\frac{A(TE)}{A(0)}\right) = -\int_0^{TE} \left(k(t') - 2H\left(t' - \frac{TE}{2}\right)k\right)^T D\left(k(t') - 2H\left(t' - \frac{TE}{2}\right)k\right) dt', \quad [6]$$

where $H(t)$ is the unit Heaviside function and $k = k(TE/2)$.[1]

From Eq. [6], Tanner defined a scalar diffusion coefficient for heterogeneous media, D^{eff}, that is averaged over the echo time, TE (19). The relationship between the effective diffusivity and the logarithm of the echo intensity can be written as

$$ln\left(\frac{A(TE)}{A(0)}\right) = -bD^{eff} \quad [7]$$

where the scalar b-factor [13] is defined as:

$$b = \int_0^{TE} \left(k(t') - 2H\left(t' - \frac{TE}{2}\right)k\right)^T \left(k(t') - 2H\left(t' - \frac{TE}{2}\right)k\right) dt'. \quad [8]$$

[1] We have elected to use the quantity k, which is more familiar to the imaging community than F, which was originally used by Stejskal and Tanner (1).

Moreover, for homogeneous, anisotropic media, Stejskal and Tanner related $A(\mathrm{TE})$, to the diffusion tensor, $\underline{D}$ (11):

$$ln\left(\frac{A(\mathrm{TE})}{A(0)}\right) = -\int_0^{\mathrm{TE}} \left(k(t') - 2H\left(t' - \frac{\mathrm{TE}}{2}\right)k\right)^{\mathrm{T}} \underline{D}\left(k(t') - 2H\left(t' - \frac{\mathrm{TE}}{2}\right)k\right) dt'. \quad [9]$$

Recently, we defined an *effective* diffusion tensor, $\underline{D}^{\mathrm{eff}}$, that is also averaged over the echo time, TE (14,20). Moreover, we showed that Eq. [9] could be rewritten as a linear relationship between the logarithm of the echo intensity and each component of $\underline{D}^{\mathrm{eff}}$ (14,20):

$$ln\left(\frac{A(\mathrm{TE})}{A(0)}\right) = -\sum_{i=1}^{3}\sum_{j=1}^{3} b_{ij}D_{ij}^{\mathrm{eff}} \quad [10]$$

where b_{ij} are elements of the b-matrix, $\underline{b}$ (14,20):

$$\underline{b} = \int_0^{\mathrm{TE}} \left(k(t') - 2H\left(t' - \frac{\mathrm{TE}}{2}\right)k\right) \left(k(t') - 2H\left(t' - \frac{\mathrm{TE}}{2}\right)k\right)^{\mathrm{T}} dt'. \quad [11]$$

The role that the b-matrix (Eq. [11]) plays in NMR studies of anisotropic diffusion is analogous to the role that the scalar b-factor (Eq. [8]) plays in NMR studies of isotropic diffusion. Diagonal elements of b_{ij} subsume the interactions between diffusion and/or imaging gradient pulses along the same direction, including "cross-terms" (21,22), while off-diagonal elements of b_{ij} couple imaging and/or diffusion gradients in *perpendicular* directions. Interactions between these orthogonal gradients had not previously been considered in NMR diffusion spectroscopy or imaging.

MEASUREMENT OF $\underline{D}^{\mathrm{eff}}$

A Gedanken Experiment

The form of Eq. [10] suggests an experiment to measure $\underline{D}^{\mathrm{eff}}$. In principle, we can infer $\underline{D}^{\mathrm{eff}}$ from a series of measured echoes using diffusion gradients applied in various oblique (noncollinear) directions. For example, in a *spectroscopic* experiment, the echo attenuation caused only by D_{xx}^{eff} can be produced by applying a gradient pulse sequence in which G has a component only in the x-direction (so that only $b_{11} = b_{xx} \neq 0$). Then,

$$\ln\left(\frac{A(\mathrm{b})}{A(0)}\right) = -b_{xx}D_{xx}^{\mathrm{eff}}. \quad [12]$$

Alternatively, the echo attenuation caused by all components of $\underline{D}^{\mathrm{eff}}$ (both diagonal and off-diagonal) can be produced by applying a gradient pulse sequence in which all three components of G are nonzero, so that

$$\ln\left(\frac{A(\mathrm{b})}{A(0)}\right) = -(b_{xx}D_{xx}^{\mathrm{eff}} + b_{yy}D_{yy}^{\mathrm{eff}} + b_{zz}D_{zz}^{\mathrm{eff}} + (b_{xy} + b_{yx})D_{xy}^{\mathrm{eff}} + (b_{xz} + b_{zx})D_{xz}^{\mathrm{eff}} + (b_{yz} + b_{zy})D_{yz}^{\mathrm{eff}}). \quad [13]$$

By applying diffusion sensitizing gradients in at least six independent oblique directions and measuring the resulting echo attenuation, we should be able to uniquely specify each element of $\underline{D}^{\mathrm{eff}}$ as well as the T_2-weighted signal, $A(0)$.

For gradient pulse sequences used in diffusion spectroscopy, simple analytic expressions can be derived for each element of the b-matrix, b_{ij}. For example, for symmetric trapezoidal pulses,

$$b_{ij} = \gamma^2 G_i G_j \left(\delta^2\left(\Delta - \frac{\delta}{3}\right) + \frac{\epsilon^3}{30} - \frac{\delta\epsilon^2}{6}\right), \quad [14]$$

where, δ is the time between the initial rise of the trapezoidal pulse and the end of its plateau; Δ is the time between the initial rise of the first and second pulses; ϵ is the rise time of the ramp; and G_i is the maximum value of the magnetic field gradient along the x_i coordinate direction (14). Mattiello et al. (23) proposed formulas for other commonly used gradient pulse sequences in spectroscopy (e.g., rectangular and sinusoidal). Moreover, for spectroscopic pulses, we can generally use Eqs. [13] and [14] to express the echo attenuation, $A(\underline{b})$, as a quadratic form of $\underline{D}^{\mathrm{eff}}$. For example, for symmetrical trapezoidal pulses:

$$ln\left(\frac{A(G,\delta,\Delta,\epsilon)}{A(0)}\right) = -\gamma^2\left(\delta^2\left(\Delta - \frac{\delta}{3}\right) + \frac{\epsilon^3}{30} - \frac{\delta\epsilon^2}{6}\right)|G|^2\hat{x}^{\mathrm{T}}\underline{D}^{\mathrm{eff}}\hat{x}, \quad [15]$$

where now we have written the echo attenuation as a function of the various independent pulse parameters, and used the relation $G = |G|\hat{x}$, where $\hat{x}$ is a unit vector in the direction of the diffusion gradient. If the medium were isotropic with diffusivity D_0, then Eq. [15] reduces to a familiar expression for the scalar b-factor (24,25):

$$ln\left(\frac{A(G, \delta, \Delta, \epsilon)}{A(0)}\right) = -b\,D_0$$

$$= -\gamma^2 |G|^2\left(\delta^2\left(\Delta - \frac{\delta}{3}\right) + \frac{\epsilon^3}{30} - \frac{\delta\epsilon^2}{6}\right)D_0 \quad [16]$$

N.B.: In MR diffusion tensor imaging, the relationship between the measured signal and the diffusion tensor cannot be simply expressed as a quadratic form of the diffusion gradient vector, as in Eq. [15].

Estimation of $\underline{D}^{eff}$ from Echo Intensity Measurements

If measurements of the echo intensity were noise-free, then we could determine $A(0)$ and the six independent elements of the $\underline{D}^{eff}$ with only seven independent experiments (simply by inverting a 7×7 matrix constructed from Eq. [15]). Since measurements of echo intensity are noisy, this approach yields poor estimates of $\underline{D}^{eff}$, especially when the signal-to-noise ratio is small. Therefore, we perform more than seven independent trials, and estimate $\underline{D}^{eff}$ statistically. Specifically, we use multivariate linear regression (26) of Eq. [13] to estimate the components of $\underline{D}^{eff}$ in a voxel (14). The optimal $\underline{D}^{eff}$ minimizes the sum of the squares of the differences between measured and theoretically predicted spin-echo intensities. A detailed explanation of this procedure is given elsewhere (14).

In general, we choose $n \geq 7$ noncollinear gradient directions[2]. We make m measurements of $A(G)$ at different gradient strengths. These nm observations of $ln(A(G))$ are stored as an $nm \times 1$ column vector, x. We define another column vector of parameters to be extimated, α, which has seven elements—the six diffusion coefficients and $ln(A(0))$:

$$\alpha = (D_{xx}^{eff}, D_{yy}^{eff}, D_{zz}^{eff}, D_{xy}^{eff}, D_{xz}^{eff}, D_{yz}^{eff}, ln(A(0)))^T. \quad [17]$$

Next, we express an $nm \times 1$ column vector of predicted outcomes as the product of an $nm \times 7$ matrix, B (computed from Eq. [13] and the b-matrix for each experiment) and α, and write the chi-squared parameter, $\chi^2(\alpha)$:

$$\chi^2(\alpha) = (x - B\alpha)^T \sum^{-1} (x - B\alpha), \quad [18]$$

which is the weighted sum-of-squares of deviations between the observed and predicted echo intensities. For each of the $m \times n$ independent trials, the squared deviation is weighted by the corrected reciprocal error variance for that measurement, x_i^2/σ_{ii}^2, which are the diagonal elements of the covariance matrix, Σ^{-1}. These diagonal elements account for the expected variation in each trial, and correct for the distortion introduced by the logarithmic transformation of $(A(G)/A(0))$ (27).

Minimizing $\chi^2(\alpha)$ with respect to each of the seven unknown parameters in α yields seven linear (normal) equations. The optimal estimated parameters, α_{opt}, are:

$$\alpha_{opt} = (B^T\Sigma^{-1}B)^{-1}(B^T\Sigma^{-1})x = M^{-1}(B^T\Sigma^{-1})x \quad [19]$$

where M^{-1} is a 7×7 matrix whose diagonal elements are the error variances of the seven estimated parameters, α_{opt}.

Alternatively, we could use nonlinear regression methods, such as the Levenberg-Marquardt algorithm, on the untransformed form of Eq. [10] relating the echo intensity and the diffusion tensor:

$$A(G) = A(0) \exp\left(-\sum_{i=1}^{3}\sum_{j=1}^{3} b_{ij}D_{ij}^{eff}\right). \quad [20]$$

In summary, we have reduced the problem of measuring $\underline{D}^{eff}$ using NMR methods to a routine problem of statistical estimation, just as Tanner [19] used Eq. [7] to estimate D^{eff} in microscopically heterogeneous but macroscopically isotropic media using weighted ~~multivariate~~ linear regression. Moreover, we do not neglect off-diagonal components of $\underline{D}^{eff}$ *a priori* (i.e., we do not constrain them to be zero), as others have. Instead, we assume that each component of $\underline{D}^{eff}$ may contribute to the measured echo intensity (as in Eq. [13]), and we assess its importance only after $\underline{D}^{eff}$ has been estimated.

Extending Diffusion Spectroscopy to Diffusion *Tensor* Imaging

To perform diffusion tensor imaging, we imbed the spin-echo diffusion sequence into an imaging sequence. Specifically, we obtain a series of diffusion-weighted images by applying diffusion sensitizing gradients in at least seven oblique directions, just as in diffusion tensor spectroscopy. Using Eq. [11], we now calculate a b-matrix for each image off-line, either numerically or analytically, as described by Mattiello [23] and in Chapter 5. From these diffusion-weighted images, we estimate an effective diffusion tensor in each voxel. Thus, the relationship between diffusion *tensor* spectroscopy and diffusion *tensor* imaging is analogous

[2] In principle, one can apply field gradients in six noncollinear directions and perform one trial with all diffusion gradients set to zero, as others have done. This method typically fails in spectroscopy, because when $G = 0$, the measured echo is often contaminated by the FID that is usually suppressed by the "crushing" effect of the diffusion gradients.

to the relationship between diffusion spectroscopy and diffusion imaging. Just as Le Bihan and others used Eqs. [7] and [8] to estimate D^{eff} within each voxel, which they called MR diffusion imaging (21,28), we use Eqs. [4], [5], [10], and [11] to estimate $\underline{D}^{eff}$ in each voxel, which we call MR diffusion *tensor* imaging.

APPLICATIONS OF DIFFUSION TENSOR IMAGING

The Principal Coordinate Axes and Principal Diffusivities

For each estimated $\underline{D}^{eff}$, whether it is measured for an entire tissue sample or for an individual voxel, we can construct a local orthogonal coordinate system (the principal coordinate axes) along which diffusive fluxes and concentration gradients are decoupled. Alternatively, this fiber frame is the one in which correlations between macroscopic particle displacements in orthogonal directions vanish. We also calculate three diffusion coefficients in these three principal directions (principal diffusivities). Because $\underline{D}^{eff}$ is symmetric and positive definite, its three eigenvectors (principal coordinate directions), ϵ_1, ϵ_2, and ϵ_3, are orthogonal. Related to them are three positive eigenvalues (principal effective diffusivities), λ_1, λ_2, and λ_3 that satisfy:

$$\underline{D}^{eff}\epsilon_i = \lambda_i\epsilon_i \quad \text{for} \quad i = \{1, 2, 3\}. \qquad [21]$$

The three equations in Eq. [21] can be rewritten in matrix form as

$$\underline{D}^{eff}\underline{E} = \underline{E}\,\underline{\Lambda} \text{ with } \underline{E} = (\epsilon_1 \mid \epsilon_2 \mid \epsilon_3) \text{ and}$$

$$\underline{\Lambda} = \begin{pmatrix} \lambda_1 & 0 & 0 \\ 0 & \lambda_2 & 0 \\ 0 & 0 & \lambda_3 \end{pmatrix}, \qquad [22]$$

where $\underline{\Lambda}$ is the diagonal matrix of eigenvalues and $\underline{E}$ is the matrix of orthonormal eigenvectors, arranged in columns.

As suggested above, in media such as brain white matter and skeletal muscle, the macroscopic anisotropy described by $\underline{D}^{eff}$ at a macroscopic (voxel) length scale is due to microscopic heterogeneity—primarily ordered semipermeable membranes, fibers, or macromolecules that retard diffusion (3). So, in anisotropic tissues, the principal directions of $\underline{D}^{eff}$ should coincide with the orthotropic directions of those structures. In particular, the eigenvector associated with the largest eigenvalue (diffusivity) defines the tissue's fiber-tract axis, while the two remaining eigenvectors, which are perpendicular to it, define the two remaining orthotropic axes.

The Effective Diffusion Ellipsoid

The effective diffusion tensor, $\underline{D}^{eff}$, inherently contains more information than a scalar ADC. Some of this information can be represented graphically by an effective diffusion ellipsoid. To motivate its use, recall that in Eq. [3] $\underline{D}^{eff}(\tau_d)$ could be interpreted as a covariance matrix of the translational displacement probability, $\rho(r \mid r_0, \tau_d)$. We can construct an effective diffusion ellipsoid by setting the quadratic form in the exponent of $\rho(r \mid r_0, \tau_d)$ in Eq. [3] to ½, i.e.,

$$\frac{(r - r_0)^T \underline{D}^{eff^{-1}}(\tau)(r - r_0)}{2\tau_d} = 1. \qquad [23]$$

The shape of the effective diffusion ellipsoid has a useful physical interpretation. If we imagine that the tissue were homogeneous and anisotropic, with a diffusion tensor $\underline{D} = \underline{D}^{eff}(\tau_d)$, then Eq. [23] defines a surface of constant mean translational displacement of spin-labeled particles at a diffusion time $t = \tau_d$. To make this explicit, we first transform[3] from the "laboratory" coordinate frame (r), in which the components of $\underline{D}^{eff}(\tau_d)$ are measured, to the "principal" or "fibers" coordinate frame (r') within a particular voxel centered at r_0, using

$$r' = \underline{E}^T(r - r_0). \qquad [24]$$

Then, using Eqs. [24] and [22], we diagonalize $(\underline{D}^{eff})^{-1}$ in Eq. [23]:

$$\frac{r'^T \underline{\Lambda}^{-1} r'}{2\tau_d} = 1. \qquad [25]$$

When expanded, Eq. [25] defines an ellipsoid:

$$\left(\frac{x'}{\sqrt{2\lambda_1\tau_d}}\right)^2 + \left(\frac{y'}{\sqrt{2\lambda_2\tau_d}}\right)^2 + \left(\frac{z'}{\sqrt{2\lambda_3\tau_d}}\right)^2 = 1. \qquad [26]$$

The ellipsoid's major axes are the mean effective diffusion distances ($\sqrt{\langle x_i'^2 \rangle} = \sqrt{2\lambda_i\tau_d}$) in the three principal (orthotropic) directions at time τ_d. Viewed from the laboratory frame, the effective diffusion ellipsoid also depicts the fiber-tract direction. Referring to Eq. [3], we can see that in "fiber" frame the displacement distribution is also locally uncorrelated. Representative diffusion ellipsoids are shown in Figs. 7 and 8.

In microscopically heterogeneous systems, the estimated effective diffusion coefficients may depend upon diffusion time. When the diffusion time is small with respect to the time to diffuse to the nearest barrier, $\Delta - \delta/3 \ll < r^2 > /D$, the effective diffusion tensor may be isotropic; and the corresponding diffusion ellipsoid would appear spherical. When the diffusion time is long, then the macroscopic molecular displacements

[3] We should also ensure that E has the properties of coordinate transformation, e.g., det(E) = 1. . . . .

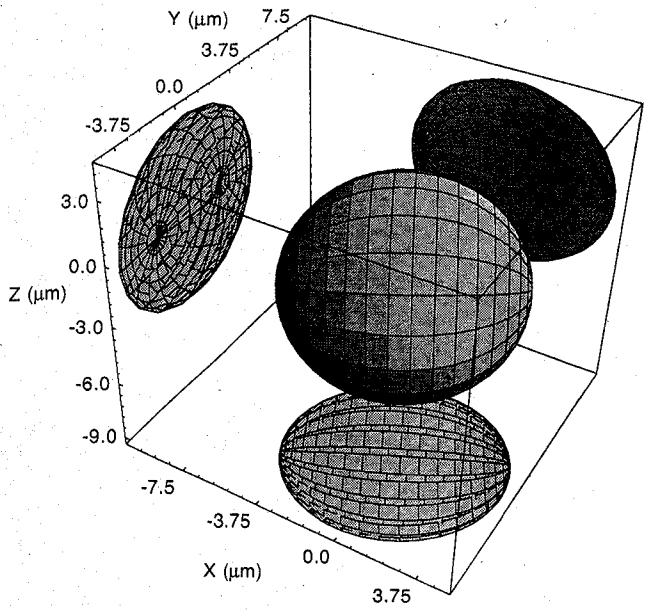

FIG. 7. Diffusion ellipsoid of a pork loin sample obtained using diffusion tensor spectroscopy. Its fiber axis is approximately aligned with the *x*-axis of the laboratory frame of reference. Laboratory coordinates *x*, *y*, and *z* are displayed in μm. The eigenvector (orthotropic direction) corresponding to the largest eigenvalue (principal diffusivity) defines the polar axis of the ellipsoid.

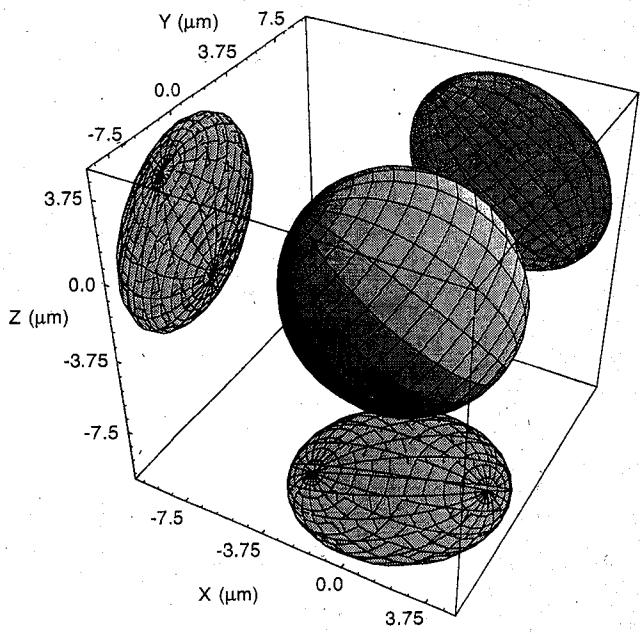

FIG. 8. Diffusion ellipsoid of the same pork loin sample shown in Fig. 7, now rotated by 41° in the *x*-*z* plane. The polar axes (i.e., fiber axes) of the diffusion ellipsoid follow the mechanical rotation of the tissue sample. This is evidenced by the tipping of the polar axis of the diffusion ellipsoid by 42° (see also Fig. 7). Both effective diffusion ellipsoids shown here and in Fig. 9 are only slightly prolate, presumably because the diffusion time, 22.5 ms, corresponds to a mean diffusion distance of only 4.7 μm, which may be too short for the spin-labeled protons to encounter diffusion barriers.

will appear anisotropic and the diffusion ellipsoid would become more prolate. In heterogeneous tissues like muscle, we might expect $\underline{D}^{\text{eff}}(\tau_d)$ to be isotropic for very short diffusion times, until a significant number of protons encounter diffusional barriers (19). However, for media with impermeable barriers, the Gaussian displacement distribution assumed above would not be adequate (29).

Scalar Invariants of $\underline{D}^{\text{eff}}$

Perhaps more important than identifying fiber direction is identifying quantities that are independent of it. Three scalar quantities that possess this property are the invariants I_1, I_2, and I_3 (30) associated with $\underline{D}^{\text{eff}}$ in each voxel. They are functions only of the eigenvalues (principal diffusivities) of $\underline{D}^{\text{eff}}$:

$$I_1 = \lambda_1 + \lambda_2 + \lambda_3 = \text{Tr}(\underline{D}^{\text{eff}}) = \text{Tr}\,(\underline{\Lambda}); \quad [27a]$$

$$I_2 = \lambda_1\lambda_2 + \lambda_3\lambda_1 + \lambda_2\lambda_3; \quad [27b]$$

$$I_3 = \lambda_1\lambda_2\lambda_3 + |\,\underline{D}^{\text{eff}}\,| = |\,\underline{\Lambda}\,|. \quad [27c]$$

These scalar quantities I_1, I_2, and I_3 are invariant with respect to rotation of the coordinate system and consequently are independent of the choice of the laboratory reference frame in which $\underline{D}^{\text{eff}}$ is measured, or equivalently, the orientation of the sample within the magnet.

These quantities have the same values irrespective of the relative orientation of the "laboratory" and "fiber" frames of reference. In addition, they are insensitive to the scheme by which the eigenvalues of $\underline{D}^{\text{eff}}$ are ordered (or numbered). As such, these invariants measure intrinsic properties of the medium, such as mean proton mobility, and have been predicted to be useful in characterizing the local microstructure and microdynamics within anisotropic tissues (15,31). Moreover, they (or functions of them) are readily measured and monitored.

Ratios of the principal diffusivities are the most natural indices of the degree of diffusion anisotropy. These dimensionless anisotropy indices measure the ratio of the effective diffusivities both parallel to and perpendicular to the fiber-tract directions. For example, one dimensionless anisotropy ratio, λ_2/λ_3, measures the rotational symmetry of the diffusion ellipsoid around the longest (fiber) axis (with $\lambda_2/\lambda_3 = 1$ indicating perfect rotational symmetry), while λ_1/λ_2 and λ_1/λ_3 measure the relative magnitude of the diffusivities in the fiber and transverse directions, and thus the eccentricity of the diffusion ellipsoid. These definitions embody our intuitive notion that an anisotropy index is a characteristic of the tissue and should be independent of the

sample's placement or orientation with respect to the (laboratory) x-y-z reference frame. An anisotropy ratio proposed by Douek et al. (3), defined as the quotient of two diagonal elements of the diffusion tensor (e.g., D_{xx}/D_{zz}) would be expected to vary as the sample is rotated (20). This deficiency is shared by an anisotropy ratio recently proposed by van Gelderen et al. (32).

Experimental Results

Diffusion tensor spectroscopy and imaging have been performed on a variety of platforms and on various media, including water, pork loin, gels, and *ex vivo* cat brain (Figs. 7 and 8). Diffusion tensor imaging was performed using FT spin-echo and echo-planar imaging sequences (12) on the same samples (Figs. 9–11). These experiments are described elsewhere (14–16,20,31,33,34). We also demonstrated the feasibility of *in vivo* diffusion tensor imaging by acquiring a sufficient number of diffusion-weighted echo-planar images (12) in under 30 minutes to construct diffusion ellipses, and invariant images (33,34). Figure 12 (*top left*) shows a proton image of lateral ventricles and corpus callosum in living human brain, acquired using EPI.

The multivariate linear model (Eq. [10]) was found to fit both diffusion spectroscopy data sets faithfully (14). In addition, the diffusivity, D_0 (in Eq. [30]), estimated by assuming water is isotropic and homogeneous, is close to published values at 14.7°C (13). Moreover, while individual elements of $\underline{D}^{eff}$ estimated for pork loin (in Eq. [31] and [32]) may differ by hundreds of percent, the eigenvalues and scalar invariants of $\underline{D}^{eff}$ differed by no more than one percent. This is what we expect since the invariant quantities reflect intrinsic properties of the medium (e.g., the trace of $\underline{D}^{eff}$ is proportional to the mean water mobility). These invariant quantities reflect microstructural and/or microdynamic changes within the tissue, but should not be affected by the sample's orientation within the magnet, suggesting their potential utility as MR imaging parameters (15). In Fig. 11, we show an image of $Tr(\underline{D}^{eff})$ for *ex vivo* cat brain. Principal diffusivities and the scalar invariants may provide additional information with which to segment tissue types. The effective diffusion ellipsoids shown in Fig. 10 are constructed in 16 × 16 voxels from the same tissue sample.

Although it is well known that the ADC varied as an anisotropic sample was rotated with respect to the direction of the applied magnetic field gradient (2), suggesting anisotropic diffusion, only the diagonal elements of the apparent diffusion tensor, D_{xx}, D_{yy}, and D_{zz}, were ever considered in diffusion spectroscopy and imaging experiments (1–4,12,35). To date, diffusion imaging of anisotropic media consisted of applying diffusion sensitizing gradients in one of three orthogonal directions, x, y, or z (as measured in the laboratory frame of reference) and estimating an ADC in each of these three directions. In NMR imaging studies, these ADCs were sometimes identified as the diagonal elements of a diffusion tensor, D_{xx}, D_{yy}, or D_{zz} [1,3,12,36,37], while off-diagonal elements of $\underline{D}^{eff}$ were not considered. However, from Eq. [10] and measured data, we see that contributions from off-diagonal elements of $\underline{D}^{eff}$ arising from interactions between imaging and/or diffusion gradients in both *parallel and perpendicular* directions can contribute significantly to the measured signal intensity.

Serious errors are made in estimating $\underline{D}^{eff}$ when its off-diagonal elements are not considered (23) both in spectroscopy and in imaging. First, one is precluded from determining a material's orthotropic axes, in particular its fiber orientation (15), because in estimating $\underline{D}^{eff}$, ignoring its off-diagonal elements is tantamount to assuming that the principal axes (eigenvectors) of $\underline{D}^{eff}$ are aligned with the x-y-z coordinate axes of the laboratory frame of reference, and that the principal diffusivities (eigenvalues) of $\underline{D}^{eff}$ are equal to the diagonal elements of $\underline{D}^{eff}$. In MR imaging, these conditions are virtually impossible to satisfy, since one seldom knows the fiber directions within an anisotropic biological or nonbiological specimen *a priori*, and these fiber

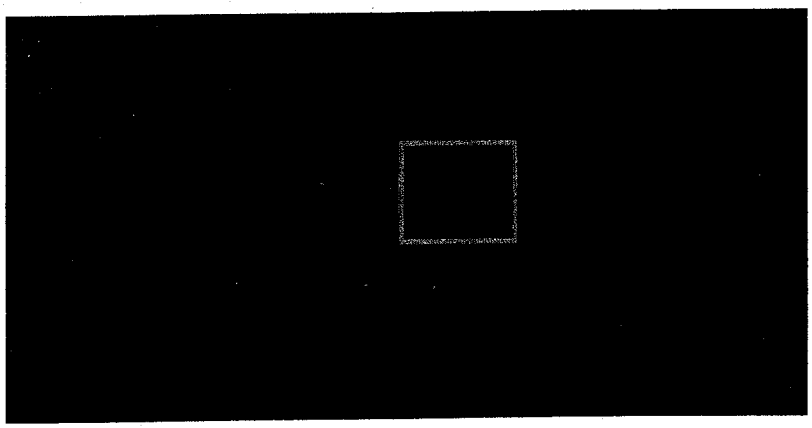

FIG. 9. A raw proton image of a sagittal section of an excised cat brain with the cerebellum at the top. The box encloses a (16 × 16 pixel) region of interest containing a portion of the corpus callosum and a ventricle filled with CSF. For this ROI, we estimated an effective diffusion tensor in each voxel.

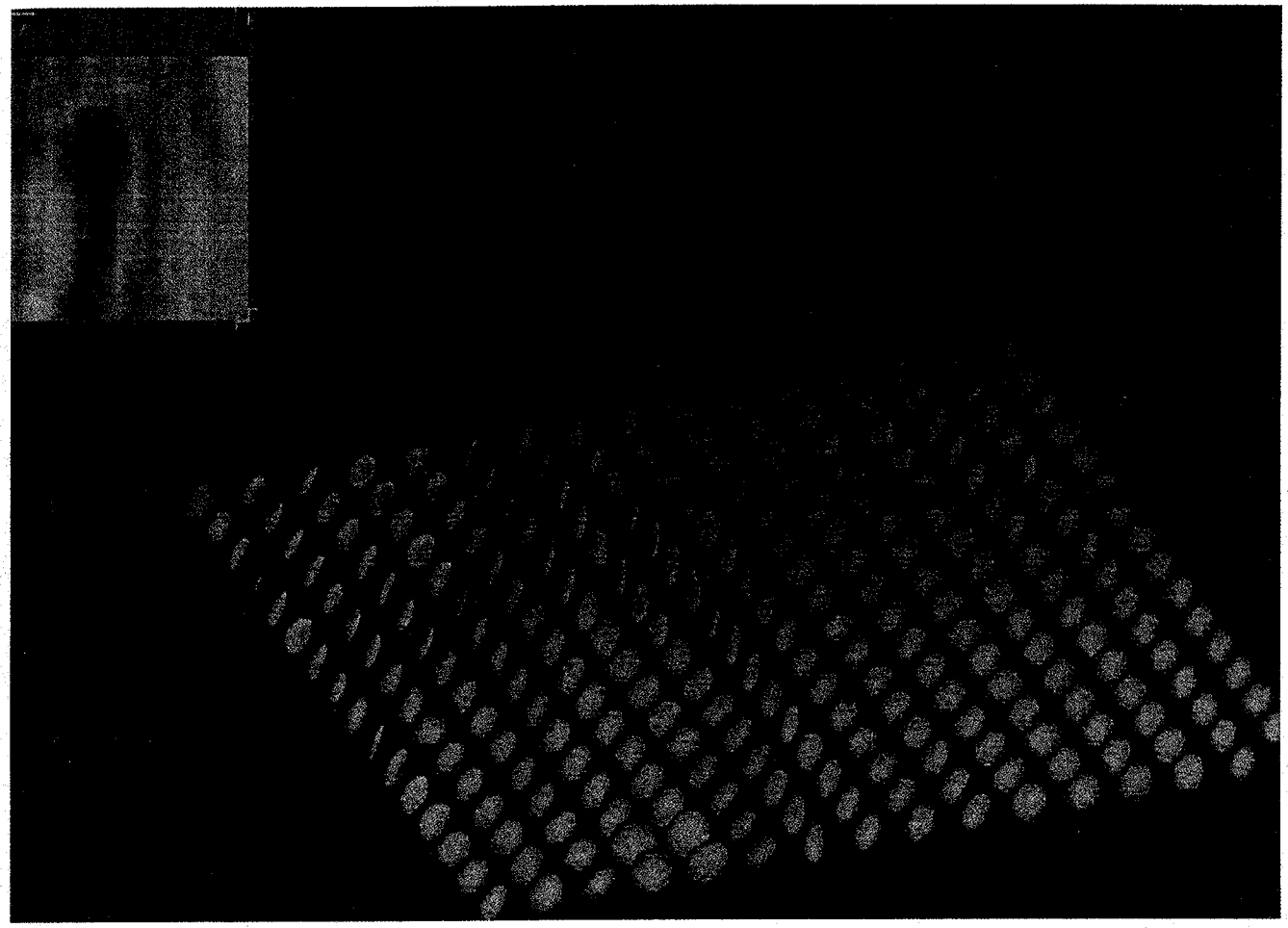

FIG. 10. Effective diffusion ellipsoid image of the ROI shown in Fig. 9. The 16 × 16 array of ellipsoids is displayed above as a gray scale image of the first scalar invariant of the effective diffusion tensor, $Tr(\underline{D}^{eff})$. Juxtaposed is an image of the effective diffusion ellipsoids that were constructed from $\underline{D}^{eff}$ estimated in each of the 16 × 16 corresponding voxels. Their shapes are consistent with known tissue composition and fiber orientation in this region of brain tissue. For example, the fibers within the corpus callosum are properly oriented (i.e., they correlate with known anatomy), while a ventricle filled with CSF is depicted by a large spherical ellipsoid indicating isotropic diffusion. Gray and white matter are also easily distinguished. Moreover, spatial gradients in fiber-tract orientation on a multi-voxel length scale are also seen.

FIG. 11. Image of the first scalar invariant, $Tr(\underline{D}^{eff})$, calculated for the same sagittal section of excised cat brain shown in Fig. 9. The box indicates the ROI from which the diffusion ellipsoids were constructed in Fig. 10. $Tr(\underline{D}^{eff})$ provides information not contained in the raw image shown in Fig. 9. For example, it is relatively easy to distinguish regions of CSF, gray and white matter, fissures, and the corpus callosum.

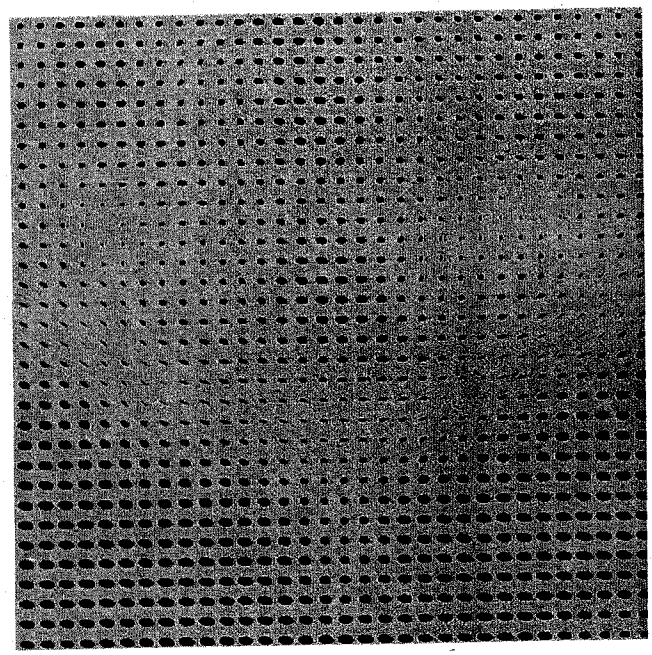

FIG. 12. Diffusion ellipse image of lateral ventricles and corpus callosum in living human brain, acquired using EPI. The diffusion ellipse image constructed from $\underline{D}^{eff}$ is the projection of the diffusion ellipsoid image onto the coronal plane. The larger ellipses indicate fluid in the ventricular space, while the highly organized, small ellipses indicate white matter fiber tracts in the corpus callosum.

directions invariably change within the field of view. Second, by ignoring off-diagonal elements of $\underline{D}^{eff}$, one incorrectly estimates $\underline{D}^{eff}$, precluding the accurate estimation of functions derived from it, such as the trace of $\underline{D}^{eff}$. For example, the ADCs one estimates from diffusion-weighted images by applying diffusion-sensitizing gradients in each of the three perpendicular directions, ADC_x, ADC_y, ADC_z, are generally not equal to the diagonal elements of the effective diffusion tensor, D_{xx}^{eff}, D_{yy}^{eff}, and D_{zz}^{eff}, respectively (15), contrary to recent claims (32). Therefore, there is no basis for the claim that $ADC_x + ADC_y + ADC_z$ possesses the desirable rotational invariance that the trace of $\underline{D}^{eff}$ does (31).

Hardware Tuning Using Diffusion Tensor Measurements

We have also proposed the use of $\underline{D}^{eff}$ to correct measurement errors caused by misalignment and improper scaling of the time-dependent B-field gradients used in diffusion NMR imaging and spectroscopy. Because the effective diffusion tensor is estimated from an equation (e.g., Eq. [15]) whose b-matrix elements scale with $|G|^2$, $\underline{D}^{eff}$ is inherently more sensitive to the magnetic field gradient than is the phase, which depends only on $|G|$. A process, formally equivalent to "whitening" of signals (38), potentially can improve the accuracy of diffusion NMR spectroscopy and imaging (15), both in the initial installation of magnetic field gradients and in the subsequent interpretation of spin-echo signals in diffusion spectroscopy and imaging.

Moreover, we hope to maximize the information gain per experiment by improved statistical estimation methods and experimental design.

CONCLUSION

We have described a method to estimate the components of $\underline{D}^{eff}$ in a voxel from spin-echo experiments. In contrast to diffusion MRI, diffusion *tensor* MRI inherently contains higher-order *intravoxel* microstructural and microdynamic information. The eigenvectors of $\underline{D}^{eff}$ can be used to construct a local frame of reference within a voxel (which we associate with the local orthotropic directions of the medium); and the eigenvector of the largest eigenvalue defines the local fiber-tract axis. The eigenvalues of $\underline{D}^{eff}$ are the diffusion coefficients in these orthotropic directions. The effective diffusion ellipsoid displays the mean diffusion distances along each of the three principal directions at a diffusion time defined by the gradient pulse sequence. The three scalar invariants of $\underline{D}^{eff}$, which are readily measured and monitored, contain complementary information about mobility and microstructure that is independent of fiber orientation *per se*, and may reflect subtle changes in compartmental volumes, permeabilities, and viscosities.

Characterizing the $\underline{D}^{eff}$ of protons or metabolites within anisotropic media may have great potential significance. For example, in ontogeny, it would provide a means of monitoring the development of anisotropic tissues and ordered structures *in vivo*, both noninvasively and nondestructively. In physiology, it would provide a means to infer cell-membrane, intracellular, and interstitial diffusivities from an appropriate microstructural model of the tissue structure. In anatomy, it would provide a means of producing fiber-tract orientation maps, of segmenting different tissue types, and even of visualizing muscle and nerve fiber tracts individually. In pathophysiology, it may provide a means of diagnosing and monitoring the progression of various diseases, such as diffuse demyelination, ischemia (including stroke), and edema (even helping to distinguish between cytotoxic, vasogenic, and interstitial edemas). Finally, this technique can potentially be used to test nonmagnetic samples nondestructively (e.g., gels and *in vitro* cell and tissue cultures).

ACKNOWLEDGMENTS

This work was performed at the NIH *In Vivo* NMR Center. We thank Alan Olson for his technical support; Robert Turner, Philippe Douek, and Bradley Roth for their thoughtful suggestions; Barry Bowman for his meticulous editing of the manuscript; and Wolfram Jarisch and Gregory Campbell for their advice about optimal experimental design and hypothesis testing, respectively.

REFERENCES

1. Moseley ME, et al. Diffusion-weighted MR imaging of anisotropic water diffusion in cat central nervous system. *Radiology* 1990;176:439–446.
2. Cleveland GG, et al. Nuclear magnetic resonance measurement of skeletal muscle. Anisotropy of the diffusion coefficient of the intracellular water. *Biophys J* 1976;16:1043–1053.
3. Douek P, et al. MR color mapping of myelin fiber orientation. *J Comput Assist Tomogr* 1991;15:923–929.
4. Chenevert TL, et al. Anisotropic diffusion in human white matter: demonstration with MR techniques in vivo. *Radiology* 1990; 177:401–405.
5. Le Bihan D. Diffusion/perfusion MR imaging of the brain: from structure to function. *Radiology* 1990;177:328–329.
6. DeGroot SR, et al. *Non-equilibrium thermodynamics*. New York: Dover; 1984.
7. Casimir HBG. On Onsager principle of microscopic reversibility. *Rev Mod Phys* 1945;17:343–350.
8. Onsager L. Reciprocal relations in irreversible processes. Part I. *Physical Review* 1931;37:405.
9. Onsager L. Reciprocal relations in irreversible processes. Part II. *Physical Review* 1931;38:2265.
10. Stejskal EO. Use of spin echoes in a pulsed magnetic-field gradient to study restricted diffusion and flow. *Journal of Chemical Physics* 1965;43:3597–3603.
11. Stejskal EO, et al. Spin diffusion measurements: spin echoes in the presence of time-dependent field gradient. *Journal of Chemical Physics* 1965;42:288–292.
12. Turner R, et al. Echo-planar imaging of intravoxel incoherent motion. *Radiology* 1990;177:407–414.
13. Le Bihan D. Molecular diffusion nuclear magnetic resonance imaging. *Magn Reson Q* 1991;7:1–30.
14. Basser PJ, et al. Estimation of the effective self-diffusion tensor from the NMR spin-echo. *J Magn Reson* 1994; series B; 247–254.
15. Basser PJ, et al. Fiber orientation mapping in an anisotropic medium with NMR diffusion spectroscopy. In: *Abstracts of the proceedings of the eleventh annual meeting of the Society of Magnetic Resonance in Medicine*. Berkeley: Society of Magnetic Resonance in Medicine. 1992:1221.
16. Basser PJ, et al. MR imaging of fiber-tract direction and diffusion in anisotropic tissues. In: *Abstracts of the proceedings of the twelfth annual meeting of the Society of Magnetic Resonance in Medicine*, New York. Berkeley: Society of Magnetic Resonance in Medicine; 1993:1403.
17. Bloch F. Nuclear induction. *Physical Review* 1946;70:460–474.
18. Torrey HC. Bloch equations with diffusion terms. *Physical Review* 1956;104:563–565.
19. Tanner JE. Transient diffusion in system partitioned by permeable barriers. Application of NMR measurements with a pulsed field gradient. *Journal of Chemical Physics* 1978;69:1748–1754.
20. Basser PJ, et al. Diagonal and off-diagonal components of the self-diffusion tensor: their relation to and estimation from the NMR spin-echo signal. In: *Abstracts of the proceedings of the eleventh annual meeting of the Society for Magnetic Resonance in Medicine*, Berlin. Berkeley: Society for Magnetic Resonance in Medicine; 1992:1222.
21. Le Bihan D, et al. Imagerie de diffusion in-vivo par resonance magnetique nucleaire. *C R Acad Sci* 1985;301:1109–1112.
22. Neeman M, et al. Pulsed-gradient spin-echo studies in NMR imaging. Effects of the imaging gradients on the determination of diffusion coefficients. *J Magn Reson Imaging* 1990;90:303–312.
23. Mattiello J, et al. An analytical expression for the b-matrix in NMR diffusion tensor imaging and spectroscopy. *J Magn Reson* 1994;103(B):247–254.
24. Price WS, et al. Effect of nonrectangular field gradient pulses in the Stejskal and Tanner (diffusion) pulse sequence. *J Magn Reson* 1991;94:133–139.
25. Trotter CM [Thesis]. Massey University; 1980.
26. Rao CR. *Linear statistical inference and its applications*. New York: Wiley; 1965.
27. Bevington PR. *Data reduction and error analysis for the physical sciences*. New York: McGraw-Hill; 1969.
28. Merboldt KD, et al. Self-diffusion NMR imaging using stimulated echoes. *J Magn Reson* 1985;64:479–486.
29. Cory DG. Measurement of translational displacement probabilities by NMR: an indicator of compartmentation. *Magn Reson Med* 1990;14:435–444.
30. Fung YC. *A first course in continuum mechanics*. Englewood Cliffs, NJ: Prentice-Hall; 1977.
31. Basser PJ, et al. MR diffusion tensor spectroscopy and imaging. *Biophys J* 1994;66:259–267.
32. van Gelderen P, et al. Water diffusion and acute stroke. *Magn Reson Med* 1994;31:154–163.
33. Basser PJ, et al. Diffusion tensor echo-planar imaging of human brain. In: *Abstracts of the proceedings of the twelfth annual meeting of the Society of Magnetic Resonance in Medicine*, New York. Berkeley: Society of Magnetic Resonance in Medicine. 1993; 1404.
34. Basser PJ, et al. Diffusion *tensor* echo-planar imaging (DTEPI) of human brain. In: *Proceedings of the Society Magnetic Resonance in Medicine Workshop: Functional MRI of the brain*, Arlington, VA; 1993:224.
35. Fullerton GD, et al. Orientation of tendons in the magnetic field and its effect on T2 relaxation times. *Radiology* 1985;155: 433–435.
36. Moonen CTW, et al. In Vivo NMR diffusion spectroscopy. ^{31}P application to phosphorus metabolites in muscle. *Magn Reson Med* 1990;13:467–477.
37. Douek P, et al. Myelin fiber orientation color mapping. In: *Abstracts of the proceedings of the tenth annual meeting of the Society of Magnetic Resonance Medicine*. San Francisco, Berkeley: Society of Magnetic Resonance in Medicine. 1991: 919.
38. Fukunaga K. Introduction to statistical pattern recognition. New York: Academic, 1972.